Superfluid-Quasicrystal in a Bose-Einstein Condensate

Junpeng Hou, Haiping Hu, Kuei Sun, and Chuanwei Zhang*
Department of Physics, The University of Texas at Dallas, Richardson, Texas 75080-3021, USA

(Received 1 September 2017; revised manuscript received 20 December 2017; published 8 February 2018)

A quasicrystal is a class of ordered structures defying conventional classification of solid crystals and may carry classically forbidden (e.g., fivefold) rotational symmetries. In view of long-sought supersolids, a natural question is whether a superfluid can spontaneously form quasicrystalline order that is not possessed by the underlying Hamiltonian, forming "superfluid-quasicrystals." Here we show that a superfluid-quasicrystal stripe state with the minimal fivefold rotational symmetry can be realized as the ground state of a Bose-Einstein condensate within a practical experimental scheme. There exists a rich phase diagram consisting of various superfluid-quasicrystal, supersolid, and plane-wave phases. Our scheme can be generalized for generating other higher-order (e.g., sevenfold) quasicrystal states, and provides a platform for investigating such new exotic quantum matter.

DOI: 10.1103/PhysRevLett.120.060407

Introduction.—Quasicrystals exhibit exotic spatial patterns that are neither periodic as solid crystals (i.e., lack of translational symmetry) nor totally disordered (i.e., possession of long-range order) [1]. The Bragg diffraction peaks of quasicrystals possess rotational symmetries such as five-, seven-, eight-, nine-, tenfold that are forbidden in classical crystalline orders [1,2]. Since its first report in Al-Mn and Al-Mn-Si alloys in 1984 [3], quasicrystal order has been studied and discovered in many different materials [4–10].

Supersolid, another exotic phase of matter, combines solid crystalline structure with superfluidity, where two continuous symmetries, namely, translational and $U(1)$ gauge, are spontaneously broken [11]. Supersolids were first predicted for helium almost 50 years ago [12,13], and have recently been observed in cold atom experiments [14,15], where a stripe phase with supersolid properties was generated and observed in a Bose-Einstein condensate (BEC) [14]. These great advances in the study of supersolids raise a natural question: Is it possible to create a novel quantum matter where both superfluidity and quasicrystal orders coexist?

In this Letter, we address this important question by proposing a scheme to generate a stable quasicrystal ground state in a BEC. The experimental setup contains a 3D BEC confined in a 1D optical superlattice with quintuple wells (defines five pseudospin states), where neighboring wells are coupled by Raman assisted tunneling to generate an effective spin-orbit coupling (SOC) [14,16] in the perpendicular plane. The scheme utilizes natural contact interaction and can realize quasicrystals with the minimum fivefold rotational symmetry. In this new quantum state, the $U(1)$ gauge symmetry is spontaneously broken just as that in supersolid stripe phases [14,16]. However, the discrete translational symmetry, which is preserved in supersolids and leads to periodic density modulations in stripe phases [14,16], has also been broken, leaving only specified rotational symmetry. A quasicrystal order with such rotational symmetry but no periodic spatial density modulation is spontaneously formed although the underlying Hamiltonian does not possess such order. Therefore, we denote this quantum matter as "superfluid-quasicrystal." By tuning system parameters (e.g., Raman coupling strength, detuning, interaction, etc.), we show, through both variational ansatz analysis and direct simulation of the mean field Gross-Pitaevskii equation (GPE), that there exists a rich phase diagram containing various superfluid-quasicrystals, supersolids, and plane-wave phases. Our scheme can be further extended to generate any n-order superfluid-quasicrystal phases. Our results may advance our understanding of both quasicrystals and superfluids and should provide an excellent platform for exploring many interesting properties of superfluid-quasicrystals, a novel format of quantum matter.

Experimental scheme and Hamiltonian.—We consider a 3D BEC confined in a tilted superlattice potential

$$V_{\mathrm{SL}}(z) = V_1 \sin^2(k_{L1} z) + V_2 \sin^2(k_{L2} z + \phi_{12}) + \alpha_z z \quad (1)$$

along the z direction [Fig. 1(a)] with $k_{L2} = k_{L1}/5$. Here two lattices can come from the same laser source with the second lattice potential formed by two beams intersecting with an angle $\theta = 2\arcsin(1/5) \approx 23°$. The linear potential $\alpha_z z$ can be realized with a magnetic field gradient. Note that this superlattice does not defy the definition for superfluid-quasicrystal because it only breaks the translational symmetry in the z direction, while the spontaneous formation of (quasi)crystal order is on the x-y plane. We denote five wells in each unit cell as five pseudospins and the effective couplings Ω between neighboring spins are induced by five

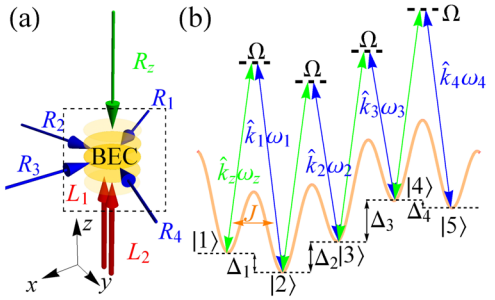

FIG. 1. (a) Proposed experimental scheme for generating superfluid-quasicrystals with fivefold rotational symmetry. The superlattice is generated by two optical lattices with different periods. A potential gradient can be generated using a magnetic field gradient. One Raman beam R_z in the z direction and four others (R_j, $j = 1, 2, 3, 4$) in the x-y plane generate the Raman coupling between neighboring wells. (b) SOC in one unit cell. Each Raman process only couples well j to its adjacent neighbor $j+1$. The hopping between neighboring unit cells is irrelevant because of the large bias between $|1\rangle$ and $|5\rangle$. Only Raman-assisted interwell tunneling in a unit cell is considered.

Raman beams, one in the z direction and four in the x-y plane with designated wave vectors $\hat{k}_j$ [Fig. 1(b)]. We choose suitable parameters ϕ_{12}, α_z such that the energy bias between neighboring wells $|\Delta_j| \gg J$ to avoid direct hopping (J is the bare tunneling rate without Raman coupling) and $||\Delta_j| - |\Delta_i|| \gg \Omega$ for $i \neq j$ so that two neighboring wells are coupled only by one specific Raman pair.

The effective single particle Hamiltonian H_0 in the x-y plane can be written as

$$H_0 = \sum_{j=1}^{5} \left(\frac{(\hat{p} - \hat{p}_j)^2}{2} + \delta_j \right) |j\rangle\langle j| + \sum_{j=1}^{4} \left(\frac{\Omega}{2} |j\rangle\langle j+1| + \text{H.c.} \right), \quad (2)$$

after a standard unitary transformation of the pseudospin phases to remove the spatial dependence of the Raman coupling [17]. Here we choose the units as $\hbar = k_R = m = 1$, where k_R is the recoil wave vector and m is atomic mass. The energy unit $E_R = \hbar^2 k_R^2/m = 1$. δ_j is the detuning determined by the Raman transition. $\hat{p}_j$ satisfying $\hat{p}_j = \hat{p}_{j-1} + 2\hat{k}_{j-1}$ and $\hat{p}_1 = -\frac{2}{5}\sum_{j=1}^{5}(5-j)\hat{k}_j$ [17]. In order to generate good superfluid-quasicrystals, we consider a regular pentagon (all minima form an equilateral polygon) with $\hat{p}_1 = (0, 1)$, $\hat{p}_2 = (-\sqrt{5/8 + \sqrt{5}/8}, (-1 + \sqrt{5})/4)$, $\hat{p}_3 = (-\sqrt{5/8 - \sqrt{5}/8}, (-1 - \sqrt{5})/4)$, $\hat{p}_4 = (\sqrt{5/8 - \sqrt{5}/8}, (-1 - \sqrt{5})/4)$, and $\hat{p}_5 = (\sqrt{5/8 + \sqrt{5}/8}, (-1 + \sqrt{5})/4)$ [see Fig. 2(a)], which can be realized using $\hat{k}_j = (\hat{p}_{j+1} - \hat{p}_j)/2$ ($j = 1, 2, 3, 4$) for four Raman lasers in the xy plane.

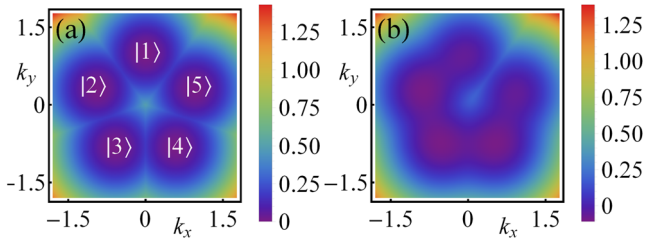

FIG. 2. Single particle lowest band dispersion. (a) $\Omega = 0$. The minima form a regular pentagon structure in the momentum space. (b) $\Omega = 0.4$. The minima are strongly coupled and all spin components are mixed. Wells 1 and 5 are uncoupled and a barrier between them can be clearly observed. The five minima are axisymmetric to $\hat{p}_3$ for any Ω.

For $\Omega = 0$ and $\delta_j = 0$ [Fig. 2(a)], five minima distribute over the vertexes of a regular pentagon. All spin components are uncoupled and only occupy one minimum. As a strong Raman coupling $\Omega = 0.4$ is ramped on [Fig. 2(b)], the minima are coupled as an open boundary chain without coupling between the head and tail. The spin components are mixed at each minimum and each well starts to merge with its adjacent neighbor. Because the locations of all minima [labeled as in Fig. 2(a)] are axisymmetric to the vector $\hat{p}_3$, the two uncoupled minima (the head and the tail) disappear first at the certain critical value of Ω (we label the remaining minima as 2 to 4). Finally, the remaining three minima merge into one (minimum 3) approximately located at $(-0.207, -0.286)$ [17] when Ω is extremely strong and its location is still along the same line as $\hat{p}_3$.

Phase diagram.—We now study new quantum phases emerging from interactions between atoms, which can be described by the GPE under the mean-field approximation with energy density

$$\epsilon = \int \frac{d\hat{r}}{V} \left[\psi^\dagger H_0 \psi + \frac{c_0}{2} n_i^2 + \frac{c_2}{2} \sum_{i=1}^{4} n_i n_{i+1} \right], \quad (3)$$

where ψ is the five-component spinor wave function, $n_i = \psi_i^\dagger \psi_i$ is the density for the spin component i, c_0 and $c_2 \approx (J/\Delta)c_0$ are the density interactions for the same and neighboring spins, respectively. For realistic parameters, $J/\Delta \sim 1/20$, the neighboring spin interaction can be ignored [14] and this is a crucial condition for realizing superfluid-quasicrystals or supersolids in experiments. The wave function is normalized by the average atomic density as $V^{-1} \int d\hat{r} \psi^\dagger \psi = \bar{n}$ with V being the system volume. We obtain the ground state using both variational ansatz analysis and direct numerical simulation of the GPE, and they agree well.

The general form of the variational ansatz is

$$\psi = \sqrt{\bar{n}} \sum_{j=1}^{5} C_j e^{i\hat{k}_{m,j}\cdot\hat{r}} \xi_j, \tag{4}$$

where C_j are complex numbers satisfying the normalization relation $\sum_j |C_j|^2 = 1$, $\hat{k}_{m,j}$ denotes each minimum in momentum space and ξ_j are the spinor part of wave function $\xi_j = (\cos\alpha_j\cos\beta_j\cos\gamma_j, \cos\alpha_j\cos\beta_j\sin\gamma_j, \sin\alpha_j, \cos\alpha_j\sin\beta_j\sin\eta_j, \cos\alpha_j\sin\beta_j\cos\eta_j)^T$. We assume $\xi_{1,j} = \xi_{5,6-j}$, $\xi_{2,j} = \xi_{4,6-j}$ ($\xi_{i,j}$ stands for the jth component of spinor ξ_i), and $\hat{k}_{m,1}(\hat{k}_{m,2})$ and $\hat{k}_{m,5}(\hat{k}_{m,4})$ are axisymmetric to vector $\hat{k}_{m,3}$ based on the symmetry of the Hamiltonian. Generally it is challenging to optimize the energy density functional with so many variables. However, in the weak interaction region $\bar{n}c_0 \ll 1$, the BEC wave function at each band minimum is quite close to the single particle spinor wave function, which can thus be used to fix ξ_j for the variational calculation. A similar method was used previously for studying a spin-1 spin-orbit coupled BEC, which gives all phases as those in full variational calculation, although the phase boundary may be slightly different for the stronger interaction [18]. We also find that $|C_1| = |C_5|$ and $|C_2| = |C_4|$ hold in weak interaction cases. The ground state energy is degenerate with respect to relative phases between C_j and the system spontaneously chooses one set of relative phases for the superfluid-quasicrystal and supersolid stripe phases.

In Fig. 3(a), we plot the phase diagram with respect to the interaction strength $\bar{n}c_0$ and Raman coupling strength Ω obtained from the variational ansatz calculation, where the color shows the occupied probability $|C_3|^2$ at the momentum minimum 3. At a finite Ω, 3 has the lowest energy; therefore, atoms only occupy 3 without interaction, leading to a plane-wave phase. On the other hand, a strong density-density interaction prefers the equal occupation of all minima. Therefore the competition between Raman coupling and interaction may render different phases, as shown in Fig. 3(a).

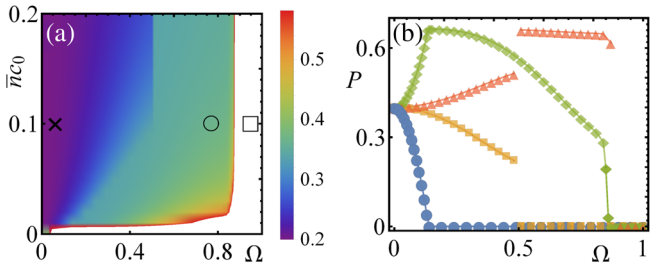

FIG. 3. (a) Phase diagram from the variational ansatz analysis when all the detunings δ_j are set to be zero. The color represents the value of $|C_3|^2$. The white region is the plane-wave phase. The three symbols (cross, circle, and square stand for $\Omega = 0.06$, 0.77, and 0.95) along $\bar{n}c_0 = 0.1$ are examples for superfluid-quasicrystal, supersolid, and plane-wave phases. (b) Phase transitions between different phases. The blue circles (green rhombus) and orange squares (red triangles) show how $|C_1|^2 + |C_5|^2$ ($|C_2|^2 + |C_4|^2$) varies with Raman coupling for $\bar{n}c_0 = 0.01$ and 0.2, respectively.

In the small Ω region, all five minima are equally populated with the same probability 1/5 due to interaction, forming a superfluid-quasicrystal [cross in 3(a)]. This new quantum matter is confirmed by the real and momentum space density distributions [Figs. 4(a) and 4(b)] obtained from the GPE simulation in a harmonic trap. We see the distribution in the real space is indeed in lack of translational symmetry, while in momentum space five equally populated peaks form a regular pentagon with each vertex designated as $\hat{p}_j$, showing the fivefold rotational symmetry of the superfluid-quasicrystal phase. Note that the harmonic trap breaks the degeneracy of the ground state and fixes the relative phases between C_j.

With the increase in Ω, the occupation of five minima changes to three, leading to a supersolid stripe phase [circle in Fig. 3(a)], where $|C_3|^2$ increases to ~0.35. The resulting real and momentum space density distributions from the GPE are shown in Fig. 4(c). Here a clear translational symmetry in the real space is observed. In the momentum space distribution (bottom inset), three minima are

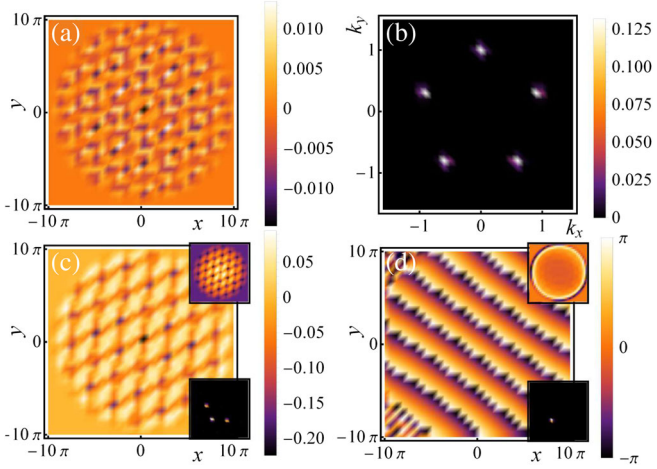

FIG. 4. (a)[(b)] Real-space (momentum-space) distribution for the superfluid-quasicrystal phase from GPE simulation. The parameters are the same as the black cross marked in Fig. 3(a). The five minima in momentum space are evenly populated. (c) Spatial distribution for a supersolid phase [parameters chosen as black circle in Fig. 3(a)] with three minima populated. The top and bottom insets show the real-space density of state $|3\rangle$ and the momentum-space distribution, respectively. (d) Phase distribution for state $|3\rangle$ at a nonzero momentum plane-wave phase, and the insets give real (top) and momentum (bottom) space distributions. The parameters correspond to the black square in Fig. 3(a). All real-space density distributions (including following panels) are obtained through subtracting the real-space density at zero Raman coupling from those of finite Ω to rule out the large density variation across the harmonic trap. The plots are rescaled over the average density in the trap. The total momentum-space distribution is the direct summation of that for each pseudospin component.

occupied unevenly and minimum 3 has a larger weight. Here Ω is quite large and the spin components in each minimum are mixed. Consequently, the spatial distribution of state $|3\rangle$ exhibits clear density modulation (top inset). For a very large Ω, all minima merge to one and the system enters a plane-wave phase [square in Fig. 3(a)]. In Fig. 4(d), we plot its phase distribution obtained from the GPE, which shows a stripe pattern as expected. The overall real space density distribution (top inset) is a Gaussian-type wave packet and the BEC occupies one point in the momentum space (bottom inset).

We characterize the transition between these phases in Fig. 3(b), where we plot the populations $P_{15} = |C_1|^2 + |C_5|^2$ and $P_{24} = |C_2|^2 + |C_4|^2$ with respect to Ω for two different interaction strengths $\bar{n}c_0 = 0.01$ and 0.2. In the weak interaction case $\bar{n}c_0 = 0.01$, P_{15} smoothly decreases to 0 and P_{24} has a sharp turn at certain Ω, showing a second-order phase transition from superfluid-quasicrystal to supersolids. This occurs when the energy bias between minima 1 and 2 with increasing Ω is larger than the interaction energy cost. For the strong interaction $\bar{n}c_0 = 0.2$, P_{15} (P_{24}) shows a sudden drop at $\Omega \sim 0.5$, showing a first-order phase transition at the point where single particle five minima merge into three. Before the transition, the interaction energy cost is so strong that P_{15} is always nonzero. Around $\Omega \sim 0.8$, the three minima merge into one and P_{24} also suddenly drops to zero, showing a first order phase transition to the plane-wave phase.

In addition to varying Ω, we may also adjust detuning δ_j to change the relative population of the minima. In Figs. 5(a) and 5(b), we plot the real and momentum-space distribution from the GPE by adding a small detuning $\delta_3 \sim 0.01E_R$ in spin state $|3\rangle$ for the superfluid-quasicrystal state in Fig 4(a). We see that the minimum 3 is now knocked out and the translational symmetry is restored. The BEC becomes a supersolid with exotic real-space distribution because it is still populated on four of five vertexes of a regular pentagon. The interplay among Raman coupling, detuning, and interaction leads to a rich phase diagram and hence enables the designing and engineering of new superfluid-quasicrystal and supersolid phases.

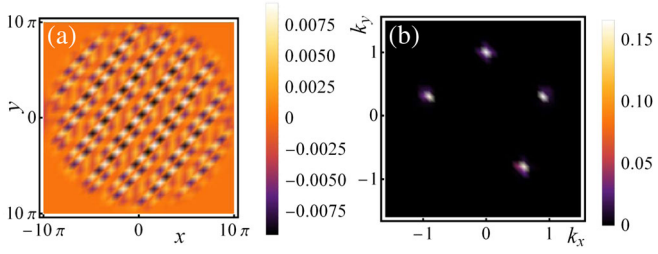

FIG. 5. (a)[(b)] Real-space (momentum-space) distribution for a supersolid phase when one minimum is knocked off with a small detuning $\delta_3 \sim 0.01E_R$ in the superfluid-quasicrystal phase in Figs. 4(a) and 4(b).

Experimental realization and detection.—The experimental realization of our scheme is in the same spirit as recent experimental reports on observing supersolid stripe phases [14,16]. Consider $N = 10^5$ ^{23}Na atoms confined in a superlattice with five wells in one unit cell and the condensate is initially split into each well equally with an average density around $\bar{n} = 0.5 \times 10^{14}$ cm^{-3}. We choose $k_R = 1064$ nm and thus $E_R = 7672$ Hz, for Raman lasers. The Raman coupling strength Ω can be tuned as low as 300 Hz [14,16], that is, $\Omega \lesssim 0.08E_R$, which well resides in the superfluid-quasicrystal region. In real experiments, $(c_0 - c_2)/c_0 \approx 1$; therefore, the neighboring-spin interaction term can be neglected. The same spin density interaction strength can be evaluated with $c_0 = 4\pi\hbar^2 a_s/m$, where a_s is the two-body scattering length. Taking $a_s = 50a_0$ (a_0 is Bohr radius) [19,20], we have $\bar{n}c_0 \approx 0.1E_R$, which is sufficiently strong for the observation of superfluid-quasicrystals, although a larger density $\bar{n}$ or scattering length a_s (tuned by Feshbach resonance) yields a larger parameter region (Fig. 3) and is better for the observation of superfluid-quasicrystal phases.

In experiments, the superfluid-quasicrystal phases may be observed in the time-of-flight (TOF) image, where five equally populated peaks are formed in the momentum space at designated positions [Fig. 4(b)]. By measuring P_{15} and P_{24} in the TOF, the quantum phase transition between different phases in Fig. 3(b) can be detected. Another way to observe the superfluid-quasicrystal phases is using Bragg scattering, similar to that for supersolids [14], where the Bragg diffraction patterns for superfluid-quasicrystals should give peaks possessing fivefold rotational symmetry [2].

Discussion and conclusion.—Our proposed experimental setup can be straightforwardly generalized for realizing other superfluid-quasicrystal phases with higher order rotational symmetry, such as $n = 7$, where 7 Raman lasers are needed with a similar experimental setup for 7 wells in a superlattice. A similar idea can also be applied to generate superfluid-quasicrystal phases in a spin-orbit coupled BEC with atomic hyperfine state pseudospins [21–33], where supersolid stripe phases have been proposed [34–44] for both 1D and 2D SOC, but have not been observed in experiments. Note that our proposed scheme for superfluid-quasicrystals requires five almost degenerate band minima for five different spins to generate a regular pentagon in the momentum space. In experiments, an effective 2D SOC (not exactly Rashba) has been experimentally realized recently [31–33] by coupling three spin states at three degenerate band minima, although the resulting band minimum path in the lowest band is not a flat ring as expected from a Rashba SOC. In our scheme, no flat Rashba ring is needed and five Raman lasers with suitable wave vectors and polarizations are chosen such that the effective band minima are formed at $\hat{p}_j$ for a regular

pentagon. The crucial difficulty comes from the interaction that is almost isotropic between any spin states. This difficulty may be resolved using ^{133}Cs atoms [45], where the interaction may be tuned by Feshbach resonance to favor the equal occupation of five minima in the momentum space, instead of the plane wave at one minimum.

In summary, we have proposed a scheme for realizing superfluid-quasicrystal stripe phases using a BEC in a 1D quintuple-well optical superlattice with Raman-assisted tunneling. Through variational and GPE analysis, we show there is a rich phase diagram containing superfluid-quasicrystals, supersolids, plane-wave phases, and their phase transitions. Our proposed experimental setup should lay out a platform for future theoretical and experimental investigations of such exotic novel quantum matter.

This work was supported by Air Force Office of Scientific Research (FA9550-16-1-0387), National Science Foundation (PHY-1505496), and Army Research Office (W911NF-17-1-0128).

*Corresponding author.
chuanwei.zhang@utdallas.edu

[1] J. Christian, *Neutron and Synchrotron Radiation for Condensed Matter Studies* (Springer, Berlin, Heidelberg, 1994).
[2] D. Levine and P. J. Steinhardt, Quasicrystals: A New Class of Ordered Structures, Phys. Rev. Lett. **53**, 2477 (1984).
[3] D. Shechtman, I. Blech, D. Gratias, and J. W. Cahn, Metallic Phase with Long-Range Orientational Order and No Translational Symmetry, Phys. Rev. Lett. **53**, 1951 (1984).
[4] E. Maciá, The role of aperiodic order in science and technology, Rep. Prog. Phys. **69**, 397 (2006).
[5] B. Freedman, R. Lifshitz, J. W. Fleischer, and M. Segev, Phason dynamics in nonlinear photonic quasicrystals, Nat. Mater. **6**, 776 (2007).
[6] K. Barkan, H. Diamant, and R. Lifshitz, Stability of quasicrystals composed of soft isotropic particles, Phys. Rev. B **83**, 172201 (2011).
[7] N. A. Wasio, R. C. Quardokus, R. P. Forrest, C. S. Lent, S. A. Corcelli, J. A. Christie, K. W. Henderson, and S. Alex Kandel, Self-assembly of hydrogen-bonded two-dimensional quasicrystals, Nature (London) **507**, 86 (2014).
[8] K. Nagao, T. Inuzuka, K. Nishimoto, and K. Edagawa, Experimental Observation of Quasicrystal Growth, Phys. Rev. Lett. **115**, 075501 (2015).
[9] J. I. Urgel, D. Écija, G. Lyu, R. Zhang, C.-A. Palma, and W. Auwärter, N. Lin, and J. V. Barth, Quasicrystallinity expressed in two-dimensional coordination networks, Nat. Chem. **8**, 657 (2016).
[10] L. Bindi, P. J. Steinhardt, N. Yao, and P. J. Lu, Natural quasicrystals, Science **324**, 1306 (2009).
[11] M. Boninsegni and N. V. Prokofv, Supersolids: What and where are they?, Rev. Mod. Phys. **84**, 759 (2012).
[12] D. J. Thouless, The flow of a dense superfluid, Ann. Phys. (N.Y.) **52**, 403 (1969).
[13] A. F. Andreev and I. M. Lifshitz, Quantum theory of defects in crystals, Sov. Phys. JETP **29**, 1107 (1969).
[14] J.-R. Li, J. Lee, W. Huang, S. Burchesky, B. Shteynas, F. Ç. Top, A. O. Jamison, and W. Ketterle, A stripe phase with supersolid properties in spin-orbit-coupled Bose-Einstein condensates, Nature (London) **543**, 91 (2017).
[15] J. Léonard, A. Morales, P. Zupancic, T. Esslinger, and T. Donner, Supersolid formation in a quantum gas breaking a continuous translational symmetry, Nature (London) **543**, 87 (2017).
[16] J. Li, W. Huang, B. Shteynas, S. Burchesky, F. Top, E. Su, J. Lee, A. O. Jamison, and W. Ketterle, Spin-Orbit Coupling and Spin Textures in Optical Superlattices, Phys. Rev. Lett. **117**, 185301 (2016).
[17] See Supplemental Material at http://link.aps.org/supplemental/10.1103/PhysRevLett.120.060407 for details about derivations of system Hamiltonian, momentum-space configuration and the nonzero momentum plane-wave phase.
[18] X.-W. Luo, K. Sun, and C. Zhang, Spin-Tensor–Momentum-Coupled Bose-Einstein Condensates, Phys. Rev. Lett. **119**, 193001 (2017).
[19] F. A. van Abeelen and B. J. Verhaar, Determination of collisional properties of cold Na atoms from analysis of bound-state photoassociation and Feshbach resonance field data, Phys. Rev. A **59**, 578 (1999).
[20] S. Knoop, T. Schuster, R. Scelle, A. Trautmann, J. Appmeier, M. K. Oberthaler, E. Tiesinga, and E. Tiemann, Feshbach spectroscopy and analysis of the interaction potentials of ultracold sodium, Phys. Rev. A **83**, 042704 (2011).
[21] Y.-J. Lin, K. Jiménez-García, and I. B. Spielman, Spin-orbit-coupled Bose-Einstein condensates, Nature (London) **471**, 83 (2011).
[22] J.-Y. Zhang, S.-C. Ji, Z. Chen, L. Zhang, Z.-D. Du, B. Yan, G.-S. Pan, B. Zhao, Y.-J. Deng, H. Zhai, S. Chen, and J.-W. Pan, Collective Dipole Oscillations of a Spin-Orbit Coupled Bose-Einstein Condensate, Phys. Rev. Lett. **109**, 115301 (2012).
[23] C. Qu, C. Hamner, M. Gong, C. Zhang, and P. Engels, Observation of Zitterbewegung in a spin-orbit-coupled Bose-Einstein condensate, Phys. Rev. A **88**, 021604(R) (2013).
[24] A. J. Olson, S.-J. Wang, R. J. Niffenegger, C.-H. Li, C. H. Greene, and Y. P. Chen, Tunable Landau-Zener transitions in a spin-orbit-coupled Bose-Einstein condensate, Phys. Rev. A **90**, 013616 (2014).
[25] C. Hamner, C. Qu, Y. Zhang, J. Chang, M. Gong, C. Zhang, and P. Engels, Dicke-type phase transition in a spin-orbit-coupled Bose-Einstein condensate, Nat. Commun. **5**, 4023 (2014).
[26] P. Wang, Z.-Q. Yu, Z. Fu, J. Miao, L. Huang, S. Chai, H. Zhai, and J. Zhang, Spin-Orbit Coupled Degenerate Fermi Gases, Phys. Rev. Lett. **109**, 095301 (2012).
[27] L. W. Cheuk, A. T. Sommer, Z. Hadzibabic, T. Yefsah, W. S. Bakr, and M. W. Zwierlein, Spin-Injection Spectroscopy of a Spin-Orbit Coupled Fermi Gas, Phys. Rev. Lett. **109**, 095302 (2012).
[28] R. A. Williams, M. C. Beeler, L. J. LeBlanc, K. Jiménez-García, and I. B. Spielman, Raman-Induced Interactions in a Single-Component Fermi Gas Near an s-Wave Feshbach Resonance, Phys. Rev. Lett. **111**, 095301 (2013).

[29] N. Q. Burdick, Y. Tang, and B. L. Lev, Long-Lived Spin-Orbit-Coupled Degenerate Dipolar Fermi Gas, Phys. Rev. X **6**, 031022 (2016).
[30] B. Song, C. He, S. Zhang, E. Hajiyev, W. Huang, X.-J. Liu, and G.-B. Jo, Spin-orbit-coupled two-electron Fermi gases of ytterbium atoms, Phys. Rev. A **94**, 061604(R) (2016).
[31] L. Huang, Z. Meng, P. Wang, P. Peng, S.-L. Zhang, L. Chen, D. Li, Q. Zhou, and J. Zhang, Experimental realization of two-dimensional synthetic spin–orbit coupling in ultracold Fermi gases, Nat. Phys. **12**, 540 (2016).
[32] Z. Meng, L. Huang, P. Peng, D. Li, L. Chen, Y. Xu, C. Zhang, P. Wang, and J. Zhang, Experimental Observation of a Topological Band Gap Opening in Ultracold Fermi Gases with Two-Dimensional Spin-Orbit Coupling, Phys. Rev. Lett. **117**, 235304 (2016).
[33] Z. Wu, L. Zhang, W. Sun, X.-T. Xu, B.-Z. Wang, S.-C. Ji, Y. Deng, S. Chen, X.-J. Liu, and J.-W. Pan, Realization of two-dimensional spin-orbit coupling for Bose-Einstein condensates, Science **354**, 83 (2016).
[34] T. D. Stanescu, B. Anderson, and V. Galitski, Spin-orbit coupled Bose-Einstein condensates, Phys. Rev. A **78**, 023616 (2008).
[35] C. Wu, I. Mondragon-Shem, and X.-F. Zhou, Unconventional Bose-Einstein Condensations from Spin-Orbit Coupling, Chin. Phys. Lett. **28**, 097102 (2011).
[36] C. Wang, C. Gao, C.-M. Jian, and H. Zhai, Spin-Orbit Coupled Spinor Bose-Einstein Condensates, Phys. Rev. Lett. **105**, 160403 (2010).
[37] T.-L. Ho and S. Zhang, Bose-Einstein Condensates with Spin-Orbit Interaction, Phys. Rev. Lett. **107**, 150403 (2011).
[38] Y. Li, L. Pitaevskii, and S. Stringari, Quantum Tricriticality and Phase Transitions in Spin-Orbit Coupled Bose-Einstein Condensates, Phys. Rev. Lett. **108**, 225301 (2012).
[39] Y. Zhang, L. Mao, and C. Zhang, Mean-Field Dynamics of Spin-Orbit Coupled Bose-Einstein Condensates, Phys. Rev. Lett. **108**, 035302 (2012).
[40] H. Hu, B. Ramachandhran, H. Pu, and X.-J. Liu, Spin-Orbit Coupled Weakly Interacting Bose-Einstein Condensates in Harmonic Traps, Phys. Rev. Lett. **108**, 010402 (2012).
[41] T. Ozawa and G. Baym, Stability of Ultracold Atomic Bose Condensates with Rashba Spin-Orbit Coupling Against Quantum and Thermal Fluctuations, Phys. Rev. Lett. **109**, 025301 (2012).
[42] K. Sun, C. Qu, Y. Xu, Y. Zhang, and C. Zhang, Interacting spin-orbit-coupled spin-1 Bose-Einstein condensates, Phys. Rev. A **93**, 023615 (2016).
[43] Z.-Q. Yu, Phase transitions and elementary excitations in spin-1 Bose gases with Raman-induced spin-orbit coupling, Phys. Rev. A **93**, 033648 (2016).
[44] G. Martone, F. Pepe, P. Facchi, S. Pascazio, and S. Stringari, Tricriticalities and Quantum Phases in Spin-Orbit-Coupled Spin-1 Bose Gases, Phys. Rev. Lett. **117**, 125301 (2016).
[45] L. W. Clark, L.-C. Ha, C.-Y. Xu, and C. Chin, Quantum Dynamics with Spatiotemporal Control of Interactions in a Stable Bose-Einstein Condensate, Phys. Rev. Lett. **115**, 155301 (2015).